Ab-initio calculations of Raman, IR-active vibrational modes in isotopically modified B_{12} icosahedral clusters

Naoyuki Nogi[a],[*], Satoru Tanaka[b]

[a]Department of Electrical and Information Engineering, Kinki University Technical College, 2800 Arima, Kumano-shi, 519-4395 Mie, Japan
[b]Department of Quantum Engineering and Systems Science, The University of Tokyo, 7-3-1 Hongo, Bunkyo-ku, 113-8656 Tokyo, Japan

Abstract

Computational calculations of Becke's three-parameter hybrid method using the LYP correlation functional (B3LYP) have been performed on $(B_{12}H_{12})^{2-}$ dodecaborane anions with different boron isotopic compositions. This was done in order to investigate isotopic dependence of vibrational spectral properties of B_{12} icosahedra, and for comparison of the optical vibrational properties of the icosahedral molecule with the characteristics of inter- or intra-icosahedral optical phonon vibrational modes in boron-rich crystals.
© 2006 Published by Elsevier Inc.

Keywords: Raman/IR-spectroscopy; B3lyp

1. Introduction

In non-metallic crystals, acoustic phonons are mainly involved in heat conduction while optical phonons are indirectly related to carrier scattering in electrical transportation. For the B_{12} icosahedral quasi-molecule, one of the subunits contained in α- or β-rhombohedral boron, vibrational properties have been previously reported [1–12]. In order to understand the mechanism of transport systems in boron-rich crystals, it is very important to consider phonon–electron (or carrier) interactions. Natural boron is composed of two stable isotopes, B-10 and B-11 with the abundance of 19.8 and 80.2 at%, respectively. Therefore, changes in the isotopic ratio of B-10 and B-11, which have a relative mass difference of 10%, are considered to have a complex effect on the thermal, electrical, and thermo-electrical functions. Therefore, as a first step, it will be illuminating to monitor the vibrational properties of the B_{12} cluster, which is the minimum unit of configuration. The isotopic configuration as an intra- (in) or inter- (between) substitutional lattice defect in subunit clusters significantly affects the optical vibrational or thermal transport properties, and the interaction of the isotope lattice defect with electro-conductive carriers needs to be considered. With regard to the B_{12} icosahedral molecule, there are no previous examples of density functional theoretical (DFT) calculations of vibrational spectral properties of the B_{12} icosahedra focused on isotopic composition or isotopic parameters, such as the boron mass number (10, 11) or nuclear spin (3, 3/2). In the present study, the characteristics of isotopic dependence affecting the vibrational spectral properties of B_{12} clusters are predicted and evaluated using DFT calculations. Using the calculated results, we can evaluate and interpret experimental data in previous reports [3] of the optical vibrational properties of natural isotopic boron.

In addition, from the viewpoint of materials engineering, we expect that the theoretical calculations will yield information on the application of isotopically controlled thin-film synthesis of the boron base for developing new solid sensors [13–15].

2. Theoretical

2.1. Computational procedure of Becke's three-parameter hybrid method using the LYP correlation functional

Using the *Gaussian* 03 quantum chemistry computational software, we performed DFT calculations using

---

*Corresponding author. Fax: +81 597 89 1018.
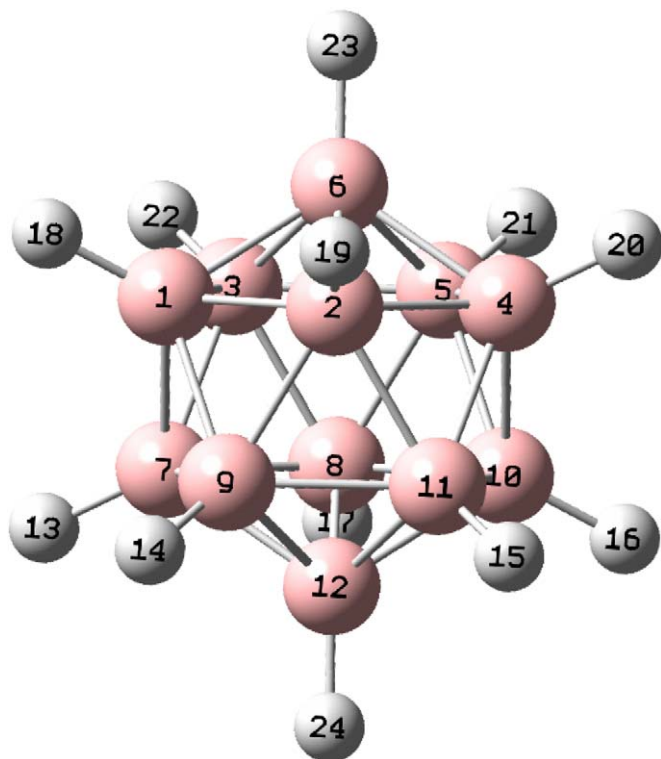*E-mail address:* nnogi@tkg.att.ne.jp (N. Nogi).

Becke's three-parameter hybrid method using the LYP correlation function (B3LYP) [16–19]. The B3LYP method has smaller errors attributable to approximations in the electron state calculations and approximation of the harmonic oscillator, as compared to the Hartree–Fock method wherein electron correlations are ignored. The B3LYP calculations were performed using the 6-31G(d) Gaussian basis set. We discuss Raman/IR-active vibrational modes by normal vibrational analysis using the $G–F$ matrix with the obtained structure energy [19]. Radom et al. have shown that the B3LYP method is excellent with regard to this point. A scaling factor of 0.9614 for the frequencies was used [20].

We performed DFT calculations for boron and hydrogen atoms using the B3LYP method on eight types of positive icosahedral $(B_{12}H_{12})^{2-}$ ions (including five types of modified ^{10}B and ^{11}B isotopes, natural isotopic composition (19.8 at% ^{10}B + 80.2 at% ^{11}B) in Table 1(A), and two types of H and T = ^3H, in Table 1(B)), labeled with the isotope as shown in Fig. 1. After structural optimization, Raman/IR spectral calculations were carried out to check how the isotopes in the boron clusters affected these characteristics.

3. Results and discussion

3.1. Calculated Raman/IR-active vibrational properties of boron icosahedra with different isotope compositions

Fig. 2(A) shows the spectra for six types of isotope-labeled $(B_{12}H_{12})^{2-}$ anions obtained by B3LYP calculations. Fig. 3 shows part of the Raman spectrum of $(B_{12}H_{12})^{2-}$ with the natural isotopic ratio (19.8 at% ^{10}B + 80.2 at% ^{11}B) quoted most in reports. $(^{10}B_3{}^{11}B_9H_{12})^{2-}$ in Fig. 2(A) is a molecule with an isotopic ratio close to the natural value. Compared to Fig. 3, it can be seen that the calculated spectra correlate with the experimental data for vibrational spectra of the $(B_{12}H_{12})^{2-}$ anion. In Fig. 3, the A_g mode frequency of the α-B_{12} crystal is higher than that of the isolated B_{12} cluster. This indicates that the bond energy between B_{12} clusters (inter-icosahedra) is greater than that within a cluster except for the vibrational energy of 12 hydrogen atoms. As for the Raman spectra, the difference of tens of cm^{-1} between the B_{12} icosahedron and α-B_{12} probably occurs because α-B_{12} clusters are coupled not by van der Waals forces, but by strongly covalent bonds.

Three comments can be made with respect to the spectra.

(1) When the calculated spectra of $(^{10}B_3{}^{11}B_9H_{12})^{2-}$ were compared with the measured data from previous reports, both the wave number and intensity were fairly well matched in the wave number region of 400–1000 cm^{-1}. In this work, we do not focus on the wave number region of 2000 cm^{-1} or higher, which includes the stretching mode of hydrogen.

Table 1
Types of isotope-modified $(B_{12}H_{12})^{2-}$ with arranged ^{10}B and ^{11}B isotopic composition based on the Z matrix (A) and $(^{10}B_6{}^{11}B_6H_6T_6)^{2-}$ with arranged ^{10}B, ^{11}B, H, and T isotopic compositions (B)

Types (a)–(e)	1	2	3	4	5	6	7	8	9	10	11	12
(A) Four types of isotope modified $(B_{12}H_{12})^{2-}$ with arranged ^{10}B and ^{11}B isotopic composition based on the Z matrix												
(a) $^{11}B_{12}$	11	11	11	11	11	11	11	11	11	11	11	11
(b) $^{10}B_3{}^{11}B_9$	10	11	11	11	11	11	11	11	11	11	11	11
(c) $^{10}B_5{}^{11}B_7$	10	11	10	11	10	11	11	11	10	11	11	11
(d) $^{10}B_6{}^{11}B_6$	11	10	10	10	10	10	10	10	10	10	10	10
(e) $^{10}B_{12}$	10	10	10	10	10	10	10	10	10	10	10	10
					(^{10}B......10		^{11}B......11)					
Types (f)–(g)	1	2	3	4	5	6	7	8	9	10	11	12
(B) Two types of isotope modified $(^{10}B_6{}^{11}B_6H_6T_6)^{2-}$ with arranged ^{10}B, ^{11}B, H, and T isotopic compositions based on the Z matrix												
(f) $^{10}B_6{}^{11}B_6$	10	11	11	11	10	11	10	11	10	11	11	11
T_6H_6	3	1	1	1	3	1	3	1	3	1	1	1
(g) $^{10}B_6{}^{11}B_6$	11	10	10	10	11	11	11	10	10	10	10	10
T_6H_6	1	3	3	3	1	3	1	3	1	3	3	3

^{10}B–T { (f) Polar / (g) Equatorial } $^{10}B...10$ $H...1$ $^{11}B...11$ $T(^3H)...3$

Boron atoms are represented as nos. 1–12, hydrogen atoms are represented as nos. 13–24.

Fig. 1. Numbering of boron-10, boron-11, and hydrogen atom positions on $(B_{12}H_{12})^{2-}$ borane icosahedra. Boron atoms are represented by label nos. 1–12, and hydrogen atoms are represented from nos. 13 to 24.
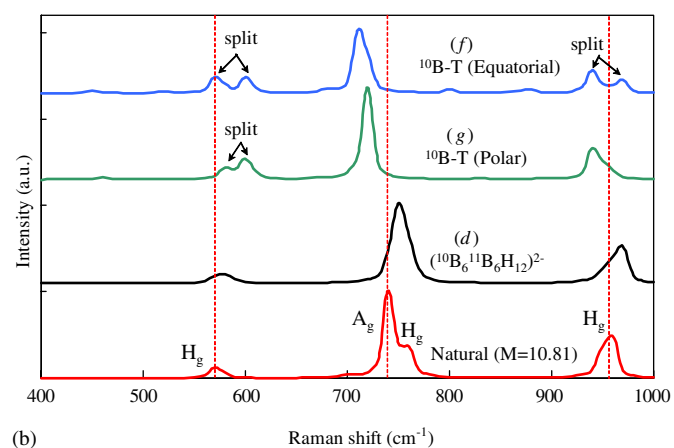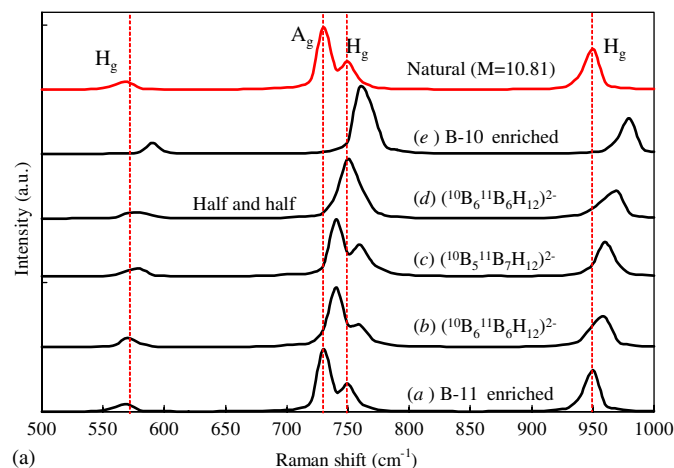

Fig. 2. (A) Raman spectra of the $(B_{12}H_{12})^{2-}$ with four different isotopic composition (a)–(d), and the natural ratio, not using isotope option by the B3LYP method (shown in Table 1(A)). (B) Calculated Raman spectra of the $\{(^{10}B_6^{11}B_6)(H_6T_6)\}^{2-}$ anion (f)–(g) with the same isotope ratio. Tritium, T, atoms were arranged in the ^{10}B atoms with a rhombohedral arrangement (f) and an equatorial arrangement (g) (shown in Table 1(B)).

(2) The spectrum in the H_g mode (around the wave number region of $750 \, \text{cm}^{-1}$) is a set of five peaks produced by mixed modes with different vibrations (see Table 2(A)). The widths and shapes of the H_g mode spectra were obtained by superposing five different peaks by the Lorentz fitting method. As a result of isotopic dependence of overlapping in each mode of H_g, the spectral shape differs depending on the isotopic composition. Since each spectrum depends on the calculation of harmonic oscillation approximation, however, this line width is not an additional wave number produced by anharmonic vibration by the isotopic distribution in B_{12}.

(3) With the vibration around $750 \, \text{cm}^{-1}$ of $(^{10}B_3^{11}B_9H_{12})^{2-}$ close to the natural isotopic ratio as the standard, ^{10}B and ^{11}B isotope-enriched molecules can be discussed. The peaks with wave numbers of 742 and $760 \, \text{cm}^{-1}$ are the breathing mode (A_{1g}) and the mixed mode (H_g), respectively. The ^{10}B-enriched B_{12} quasi-molecule has great vibrational strength because the breathing mode (A_{1g}) and mixed mode (H_g) overlap. This can be attributed to resonance by accidental degeneracy under the influence of the isotopic ratio (Fig. 4). In the case of the ^{11}B-enriched molecule, wherein A_{1g} and H_g are separated, this degeneracy can be considered to be an isotopic effect unique to the ^{10}B-enriched B_{12} quasi-molecule. As the ^{10}B ratio decreases, A_{1g} and H_g begin to separate. Only when the isotopic ratios are half-and-

half (50 at% ^{10}B + 50 at% ^{11}B), however, do the A_{1g} mode and H_g mode around the wave number of $740 \, \text{cm}^{-1}$ tend to resonate as an exception. It is interesting to note that accidental resonance occurs.

Regarding the isotopic composition of $(^{10}B)_6(^{11}B)_6H_{12}$ that has ^{10}B and ^{11}B in equal parts, tritium (T), an isotope with three times greater mass than hydrogen, was arranged close to the boron atoms with a polar site arrangement and an equatorial arrangement (Table 1(B)), and Raman shifts were calculated similarly by the B3LYP method (Fig. 2(B)). Table 2(B) shows the results for the calculations. From the results, it can be noticed that the boron-related modes are generally shifted several tens of cm^{-1} toward the low wave number side than those of the natural isotopic ratio due to the weight of tritium.

There are two interesting points to be noted regarding tritium substitution. First, the H_g mode disappears from the shoulder on the high wave number side of the A_g mode (around $700 \, \text{cm}^{-1}$), which is the breathing mode.
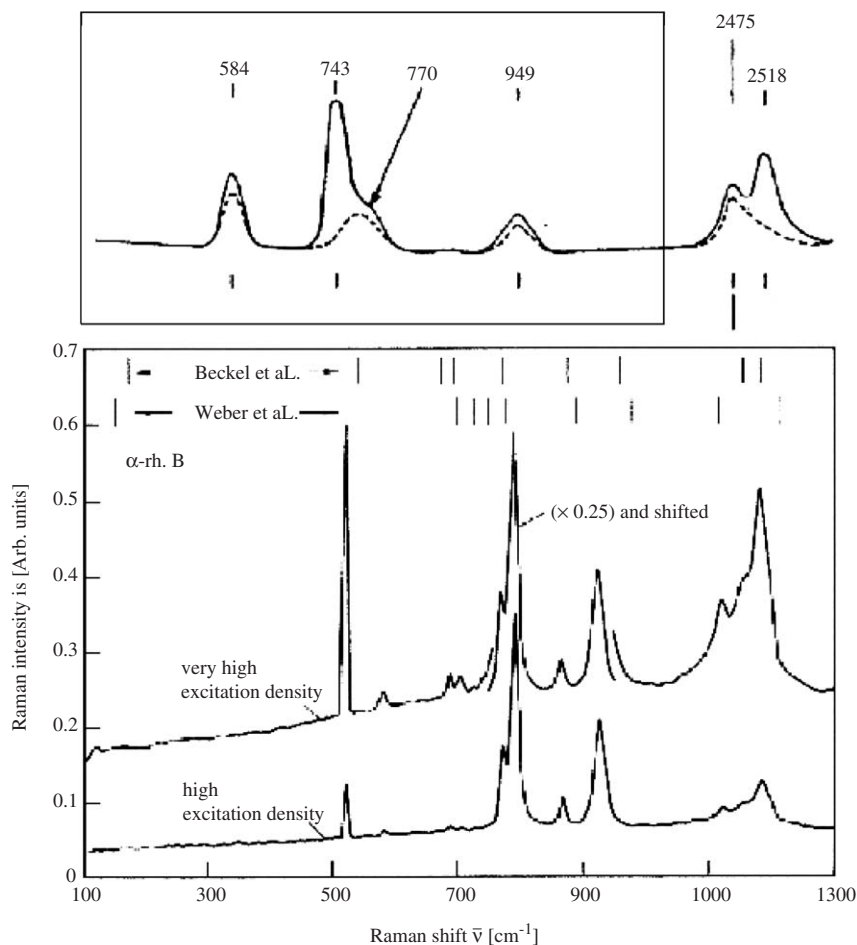
Fig. 3. Experimental data of Raman-active vibrational modes of $(B_{12}H_{12})^{2-}$ and α-B_{12} with natural isotopic composition (Ref. [3,21,22]).
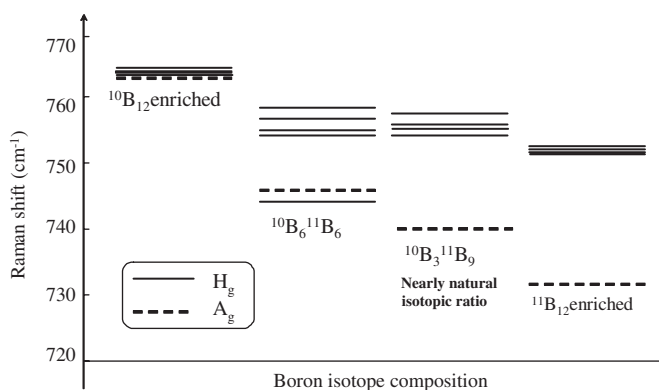

Fig. 4. Comparison of A_g, H_g modes around $740\,\mathrm{cm}^{-1}$ among $(^{10}B_{12}H_{12})^{2-}$, $(^{11}B_{12}H_{12})^{2-}$, $^{10}B_6^{11}B_6$, and $^{10}B_3^{11}B_9$ (nearly natural isotopic ratio).

This does not mean that degeneracy hides this mode, as mentioned for the ^{10}B-enriched $B_{12}H_{12}$ anion before, rather, the mode actually disappears. Secondly, the spectrum tends to split into two peaks in the H_g mode around 500 and $900\,\mathrm{cm}^{-1}$. Accompanying the isotope of B coupled with T, one mode splits into two or three groups (as shown in Table 2(B)).

Regarding the first point above, the phenomenon was seen both in the polar and equatorial arrangements. This calculation result may be related to the decrease in entropy or the high symmetry based on these isotope configurations. The second reason depends on which vibrational mode is more dominant within an H_g mode. There is a tendency to split into two symmetrical group oscillation modes. Other isotopic configurations in B_{12} need to be calculated by considering symmetry. In addition, small local spectra are scattered between the above modes.

Comparing the isotopic distribution dependence of the Raman-active spectra of the vibrations of the intra-icosahedral subunit B_{12} in the α-B_{12} crystal (Fig. 3), with the calculated Raman-active spectrum for the isolated cluster B_{12}, may help determine the characteristics of the α-B_{12} crystal in terms of isotopic distribution [21,22]. In other words, H–T substitution of the polar and equatorial sites is considered to clarify the differences in vibrational characteristics with changing isotopic distribution that occurs without changes in the molecular stability or bonding strength. Therefore, if the results of calculations, wherein the configuration of B-10 and B-11 is varied for the polar and equatorial sites, are compared with the experimental internal vibrational spectra (intra-icosahedral) of α-B_{12}

Table 2
Calculated wave number of the A_g and H_g modes around the wave number region of $740\,cm^{-1}$ (A) and of $(^{10}B_6^{11}B_6H_6T_6)^{2-}$ in the wave number region of 500–$1000\,cm^{-1}$ (B)

(A) Around the wave number region of $740\,cm^{-1}$

Freq. (cm^{-1})		Intensity (A^4/amu)	Freq. (cm^{-1})		Intensity (A^4/amu)
A_g	763	113	A_g	731	102
H_g	764	11	H_g	751	9
	765	11		752	9
	765	11		752	9
	766	11		753	9
	766	11		753	9
	^{10}B enriched			^{10}B enriched	

Freq. (cm^{-1})		Intensity (A^4/amu)	Freq. (cm^{-1})		Intensity (A^4/amu)
H_g	747	7	A_g	741	82
A_g	747	96	H_g	754	9
	756	9		754	9
	756	9		756	9
	760	10		757	9
	760	10		760	8
	^{10}B$_6$ ^{11}B$_6$ (Half and Half)			^{10}B$_3$ ^{11}B$_9$ (Nearly natural)	

(f) ^{10}B–T (Equatorial)　　　　(g) ^{10}BB–T (Polar)

(B) In the wave number region of 500–$1000\,cm^{-1}$

Freq. (cm^{-1})		Intensity (A^4/amu)	Freq. (cm^{-1})		Intensity (A^4/amu)
H_g	571	14	Hg	570	6
	575	6		571	6
	576	6		585	12
	602	11		593	11
	603	11		593	11
A_g	713	98	A_g	709	102
H_g	937	14	Hg	929	17
	940	13		930	12
	966	10		935	10
	967	10		943	2
				944	7
				945	10

using a boron crystal with a 50:50 isotopic ratio of B-10 and B-11, by repeating the optical experiment using an α-B_{12} single crystal with isotopically half and half composition, one could show whether B-10 or B-11 tends to occupy a polar site or an equatorial site of the unit cell of α-B_{12}.

The IR-active mode was calculated in the same way. In the IR-active mode, not only is the wave number deviation dependent on the mass number, in addition, a local vibration seemingly attributable to isotopic distribution was seen although its intensity was comparatively weak.

Calculations based on harmonic approximation were performed taking isotopic parameters into consideration. By comparing the experimental spectrum of the mixed mode and the spectrum consisting of a set of multiple peaks based on harmonic approximation, we found that the intensity of the specific mode in a mixed mode varies with not only the isotopic ratio but also the isotopic configuration.

With regard to the boron crystals, the rhombohedral B crystal has a B_{12} subunit structure in the unit cell. Among the thermally stable types of polymorphous, for example, β-rh. B in the rhombohedral unit cell has an element filling rate as low as 36% [23–27]. Considering not only the mass ratio with a relative difference of 10%, but their configuration of isotopes, it seems interesting to attempt experimental spectroscopy.

We feel that it is essentially important how the isotopic distribution influences the vibrational properties not only intra-icosahedron, but also inter-icosahedron as well in boron-rich solids. Currently, we have only estimated the change in vibration by modification of the hydrogen atoms at a polar site within a B_{12} cluster. Recent reports [28,29] show that the crystal structure of $B_{12}X_2$ type can be reproduced with the $(B_{12}H_{12})^{2-} + 2X^+$ sub-unit structure by considering the effect of the counter ion X^+. It seems that this treatment of $(B_{12}H_{12})^{2-}$ sub-unit clusters becomes an important clue to discuss the electronic or vibrational properties of inter-icosahedrons for boron-rich crystals. It is important to examine that this reproduction method applies to covalently bound clusters of boron-rich solids, such as α-B_{12}.

4. Conclusions

We have applied DFT calculations using the hybridizing method to $B_{12}H_{12}$ icosahedral cluster anions with different isotopic ratios. The results are summarized as follows. Using the Raman-active mode under B isotope control, we discovered an isotopic shift in the vibrational frequency by reduced mass depending on the composition of the B isotope. In particular, the A_g mode of ^{10}B showed degeneracy with the H_g mode. In the calculation of the $B_{12}T_{12}$ anion, wherein H was substituted with T, the spectral number varied not only with the isotopic composition of 12 boron atoms but also with the isotopic configuration. In this case, the H_g mode in $B_{12}H_{12}$ was found to separate into two groups. Regarding engineering

applications in devices, it is important to study how an isotope affects the interaction between the B_{12} molecular vibration and electrons. These results are expected to provide new basic knowledge for controlling the neutron absorption characteristics of boron. Computations in this work were examined using with *Gaussian* 03 quantum chemistry software and its graphical user interface, Gauss view 3.0 [30-31]

References

[1] E.L. Muetterties, R.E. Merriefield, H.C. Miller, W.H. Knoth Jr., R. Downing, J. Am. Chem. Soc. 84 (1962) 2506.
[2] J.A. Wunderlich, W.N. Lipscomb, J. Am. Chem. Soc. 38 (1960) 4427.
[3] W.H. Knoth, H.C. Miller, J.C. Sauer, J.H. Balthis, Y.T. Chia, E.L. Muetterties, J. Am. Chem. Soc. 3 (1964) 159.
[4] T.A. Green, A.C. Switendick, D. Emin, J. Chem. Phys. 89 (1988) 6815.
[5] W. Weber, M.F. Thorpe, J. Phys. Chem. Solids 36 (1975) 967.
[6] H. Werheit, H. Haupt, in: D. Emin, T. Aselage, C.L. Beckel, A.C. Switendick, B. Morosin, (Eds.), Boron-Rich Solids, Proceedings of the 10th International Symposium on Boron, Borides and Related Compounds, AIP Conf. Proc. 231 (1991) 355–359.
[7] P.A. Medwick, R.O. Pohl, J. Solid State Chem. 133 (1997) 44.
[8] H. Binnenbruck, H.Z. Werheit, Naturforschung 34a (1979) 787.
[9] T.L. Aselage, D.R. Tallant, D. Emin, Phys. Rev. B 56 (1997) 3122.
[10] D. Gabunia, O. Tsagareishvili, G. Darsavelidze, D. Lezhava, M. Antadze, L. Gabunia, J. Solid State Chem. 177 (2003) 600.
[11] H. Werheit, U. Kuhlman, N.E. Solov'ev, G.P. Tsiskarishvili, G. Tsagarcishvili, AIP Conf. Proc. 140 (1990) 350.
[12] H. Werheit, in: R. Freer (Ed.), The Physics and Chemistry of Carbides; Nitrides and Borides, Kluwer Academic Publishers, Dordrecht, 1990, pp. 705–725.
[13] M. Cardona, Physica B 376 (1999).
[14] A.A. Berezin, J. Chem. Phys. Solids 50 (1989) 5.
[15] E.E. Haller, J. Appl. Phys. 77 (1995) 2857.
[16] M.C. Payne, et al., Rev. Mod. Phys. 64 (1992) 1045.
[17] A.D. Becke, Phys. Rev. A 38 (1988) 3098.
[18] A.D. Becke, J. Chem. Phys. 98 (1993) 5648.
[19] E.B. Wilson Jr., J.C. Decius, P.C. Cross, Molecular Vibrations, McGraw-Hill, New York, 1955.
[20] A.P. Scott, L. Radom, J. Phys. Chem. 100 (1996) 16502.
[21] H. Werheit, R. Schmechel, Boron, in: O. Madelung (Ed.), Landolt-Börnstein, Numerical Data and Functional Relationships in Science and Technology, Group III: Condensed Matter, vol. 41, C, Springer, Berlin, 1998, pp. 88–89.
[22] C.L. Beckel, J.P. Vaughan, AIP Conf. Proc. 140 (1986) 305.
[23] D.F. Decker, J.S. Kasper, Acta hybridizing Crystallogr. 12 (1959) 503.
[24] B. Callmer, Acta Crystallogr. B 33 (1977) 1951.
[25] J.L. Hoard, D.B. Sullenger, C.H.L. Kennard, R.E. Hughs, J. Solid State Chem. 1 (1970) 268.
[26] S. Anderson, T. Lundström, J. Solid State Chem. 2 (1970) 603.
[27] I. Higashi, M. Kobayashi, K. Kobayashi, T. Lundström, L.E. Tergenius, T. Ito, Jpn. J. Appl. Phys. 10 (1994) 7.
[28] D.G. Allis, B.S. Hudson, J. Phys. Chem. A 110 (2006) 3744.
[29] B.S. Hudson, J. Phys. Chem. A 115 (2001) 3949.
[30] Gaussian 03, Revision B.05;
    M.J. Frisch, G.W. Trucks, H.B. Schlegel, G.E. Scuseria, M.A. Robb,

J.R. Cheeseman, J.A. Montgomery, Jr., T. Vreven, K.N. Kudin, J.C. Burant, J.M. Millam, S.S. Iyengar, J. Tomasi, V. Barone, B. Mennucci, M. Cossi, G. Scalmani, N. Rega, G.A. Petersson, H. Nakatsuji, M. Hada, M. Ehara, K. Toyota, R. Fukuda, J. Hasegawa, M. Ishida, T. Nakajima, Y. Honda, O. Kitao, H. Nakai, M. Klene, X. Li, J.E. Knox, H.P. Hratchian, J.B. Cross, C. Adamo, J. Jaramillo, R. Gomperts, R.E. Stratmann, O. Yazyev, A.J. Austin, R. Cammi, C. Pomelli, J.W. Ochterski, P.Y. Ayala, K. Morokuma, G.A. Voth, P. Salvador, J.J. Dannenberg, V.G. Zakrzewski, S. Dapprich, A.D. Daniels, M.C. Strain, O. Farkas, D.K. Malick, A.D. Rabuck, K. Raghavachari, J.B. Foresman, J.V. Ortiz, Q. Cui, A.G. Baboul, S. Clifford, J. Cioslowski, B.B. Stefanov, G. Liu, A. Liashenko, P. Piskorz, I. Komaromi, R.L. Martin, D.J. Fox, T. Keith, M.A. Al-Laham, C.Y. Peng, A. Nanayakkara, M. Challacombe, P.M.W. Gill, B. Johnson, W. Chen, M.W. Wong, C. Gonzalez, J.A. Pople, Gaussian, Inc., Pitsburgh PA, 2003.

[31] Gauss View, Version 3.0,;
Roy Dennington II, Todd Keith, John Millam, Ken Eppinnett, W. Lee Hovell, Ray Gilliland, Semichem, Inc., Shawnee Mission, KS, 2003".